Supporting Information

Carbon Nitride nanosheet supported CuO for efficient photocatalytic CO_2 reduction with 100% CO selectivity

Xingxi Lv, Xiaomeng You, Jingyi Pang, Hang Zhou, Zejiang Huang, Ye-Feng Yao, Xue-Lu Wang*

Physics Department & Shanghai Key Laboratory of Magnetic Resonance, School of Physics and Electronic Science, East China Normal University, North Zhongshan Road 3663, Shanghai 200062, P. R. China.

**Corresponding author' E-mail: xlwang@phy.ecnu.edu.cn*

Experimental

Materials

Melamine, copper nitrate trihydrate ($Cu(NO_3)_2{\cdot}3H_2O$), N,N-Dimethylformamide and ethanol were analytical grade and purchased from Sigma–Aldrich. Ultrapure water with a resistivity of 18.2 MU was used for all synthesis and photocatalytic experiments. All chemicals were of analytical grade and used without further purification. High-purity CO_2 (99.999%) was procured from Air Liquide Compressed Gas Co., Ltd. (Shanghai, China).

Synthesis of Cu_x/CN photocatalysts

Melamine (5.0 g) was dispersed in 25 mL ethanol. After continuous agitation, the suspension was transferred to a 50-mL Teflon-lined autoclave and heat-treated in water at 80 °C for 6 h. After cooling to room temperature, a precipitate was obtained via centrifugation, which was subsequently dispersed in 20 mL of ethanol and 5 mL of a copper source (1 M $Cu(NO_3)_2{\cdot}3H_2O$ ethanol solution) and stirred at 80 °C for 30 min. The resulting mixture was transferred to a 100-mL covered crucible and annealed for 2 h at a heating rate of 15 °C/min and final temperature of 550 °C and cooled to room temperature naturally inside a furnace to obtain brown powder, which was washed with ultra-pure water three times and dried under vacuum at 60 °C for 12 h. The final sample was denoted as Cu_3/CN. In addition, Cu-supported g-C_3N_4 photocatalysts with different weight fractions were synthesized at different concentrations of the $Cu(NO_3)_2$ ethanol solution (0.14, 0.6, 1.4, and 1.7 M) using the same procedure and named Cu_1/CN, Cu_2/CN, Cu_4/CN, and Cu_5/CN, respectively.

Synthesis of g-C_3N_4 photocatalyst

Bulk CN was synthesized via the polymerization of melamine (5.0 g) for 2 h at a heating rate of 15 °C/min and final temperature of 550 °C and then naturally cooled to room temperature inside the furnace.

Characterizations

The morphologies of the fabricated photocatalysts were observed via transmission electron microscopy (TEM, FEI Tecnai G2 F20) and scanning electron microscopy (SEM, Hitachi S-4800). Crystal-phase identification was performed using powder X-ray diffraction (XRD, Rigaku Ultima IV) with a Cu Kα X-ray source in the scanning range of 5–80° and scanning rate of 2° min^{-1}. Surface elemental compositions and chemical states of the prepared samples were determined via X-ray photoelectron spectroscopy (XPS, Thermo Fischer ESCALAB Xi^+). Fourier-transform infrared (FT–IR) spectra of the synthesized samples were recorded using a Thermo Fisher Nicolet Is5 infrared spectrometer in the range of 500–2500 cm^{-1} after mixing with KBr. The optical properties of all samples were evaluated through ultraviolet–visible diffusion reflectance spectroscopy (UV–vis DRS, 3010, Hitachi, Japan) in the scanning range of 200–800 nm using $BaSO_4$ as the reference. Photoluminescence (PL) and time-resolved photoluminescence (TRPL) spectra of

the fabricated samples were recorded using an F-4500 instrument (Hitachi, Japan). Cu concentrations were measured with a Thermo Scientific iCAP RQ inductively coupled plasma mass spectrometer (ICP–MS).

Photo-electrochemical characteristics

Photoelectrochemical measurements were performed in a conventional three-electrode cell configuration with a 0.5 M Na_2SO_4 aqueous solution using a CHI660E electrochemical system, in which catalyst-coated fluorine-doped tin oxide (FTO) glass, a Pt plate, and a Ag/AgCl electrode were used as the working, counter, and reference electrodes, respectively. To load a sample film electrode onto FTO glass, 5 mg of the catalyst was added to a solution containing 1 mL of isopropyl alcohol and 20 µL of Nafion. After 1 h of ultrasonication, 100 µL of the obtained solution was dropped onto FTO glass (1×1 cm^2), and the fabricated working electrode was allowed to dry at room temperature. The transient photocurrent response with an on/off switching interval of 20 s was supplied by a 300-W Xe lamp (Beijing Perfectlight Technology Co., China).

In situ FT–IR measurements

All FT–IR spectra were recorded using a Bruker Tensor II FTIR NEXUS instrument. The as-prepared sample was loaded into the cell, and the entire reaction chamber was purged with Ar for 30 min at 120 °C to blow out all gases inside the cell and species adsorbed on the sample surface. After cooling the reaction cell to room temperature, flows containing CO_2 and H_2O vapors were introduced into the reactor. The FT–IR spectra were recorded after 40 min of darkness and 70 min of irradiation.

NMR experiments

DMF (99.9%) and deuterium oxide (D_2O, 99.9% D containing 0.05 wt.% 3-23 (trimethylsilyl) propionic-2,2,3,3-d4 acid) were obtained from Sigma–Aldrich. Steps of CEST imaging experiment: 5 mg photocatalyst was dispersed in 10 ml H_2O and treated under ultrasound for 1 h, 100 mg monosodium glutamate was added with constant stirring to obtain a mixed solution. An appropriate amount of the above solution was loaded into a 5 mm capillary glass tube for testing. Subsequently, high purity CO_2 was passed into the solution for one hour and then tested again. CEST imaging experiments and DOSY NMR experiments were performed on a Bruker AVANCE III 500 MHz spectrometer. The resulting NMR spectra were processed using the Bruker TopSpin software.

Photocatalytic CO_2 reduction activity

In a typical photocatalytic CO_2 reduction reaction, 1.5 mg of a catalyst, 3 mL of H_2O, and 30 mL of DMF were added to a gas-closed quartz reactor. After evacuating the reaction system, high-purity CO_2 (99.999%) was supplied to the reactor. The temperature of the reaction system was maintained at approximately 25 °C by recirculating cooling water during irradiation. The light source for photocatalysis was a 300-W Xe lamp (Beijing Perfectlight Technology Co., China). Hydrocarbon fuel products were monitored every 20 min using a GC9790Plus gas chromatograph (Fuli, China) and flame ionization detector. To evaluate the catalyst stability, the system was vacuum-pumped after each cycle and injected with saturated CO_2 before the next cycle.

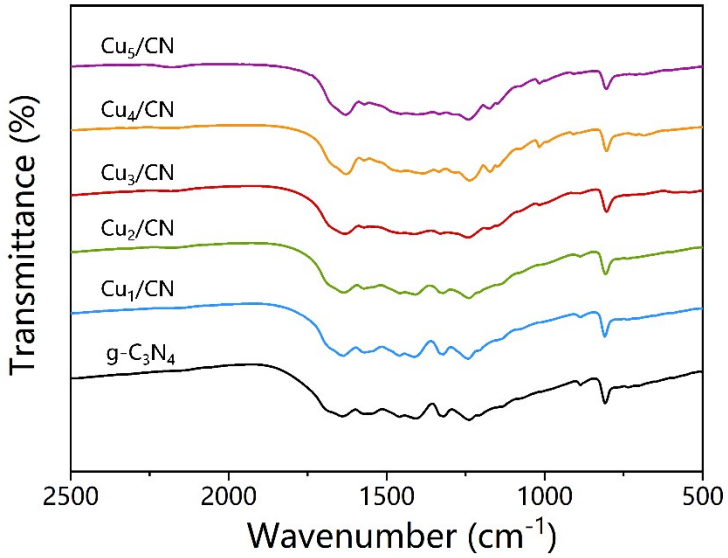

Figure S1. FT-IR spectra of g-C_3N_4 and Cu_x/CN.

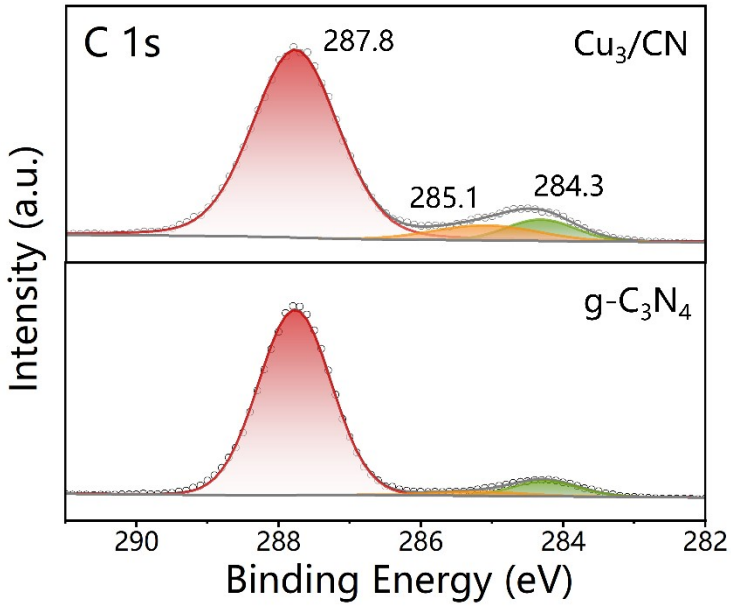

Figure S2. High-resolution XPS spectra of C 1s for g-C_3N_4 and Cu_3/CN.

The high-resolution C 1s spectrum was deconvoluted into three components with different binding energies (284.3, 285.1, and 287.8 eV), which were related to graphitic C–C bonds, the sp^3-bonded carbon of C–NH_2, and the sp^2-bonded carbons of N–C=N, respectively.

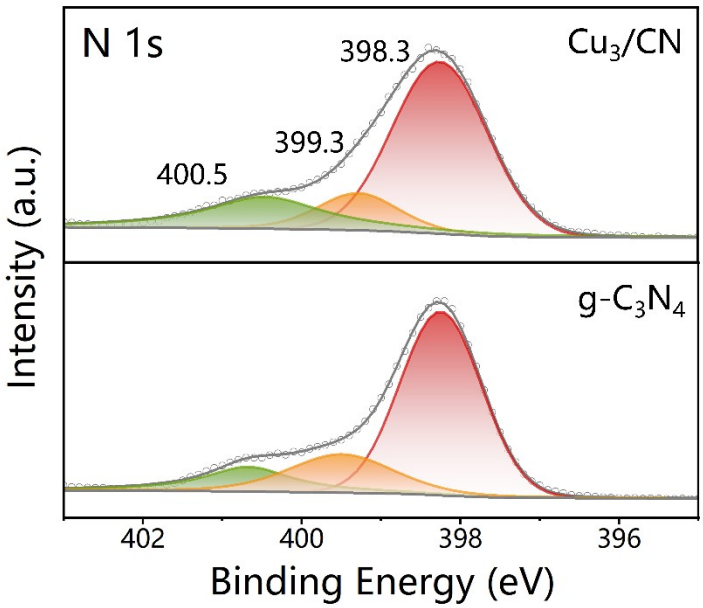

Figure S3. High-resolution XPS spectra of N 1s for g-C_3N_4 and Cu_3/CN.

The high-resolution N 1s spectrum was deconvoluted into three peaks. The first peak centered at 398.3 eV was assigned to the sp^2-hybridized nitrogen atoms (C=N–C); the peak located at 399.3 eV belonged to the tertiary nitrogen in N–$(C)_3$; and the peak centered at 400.5 eV was due to N–H bonding.

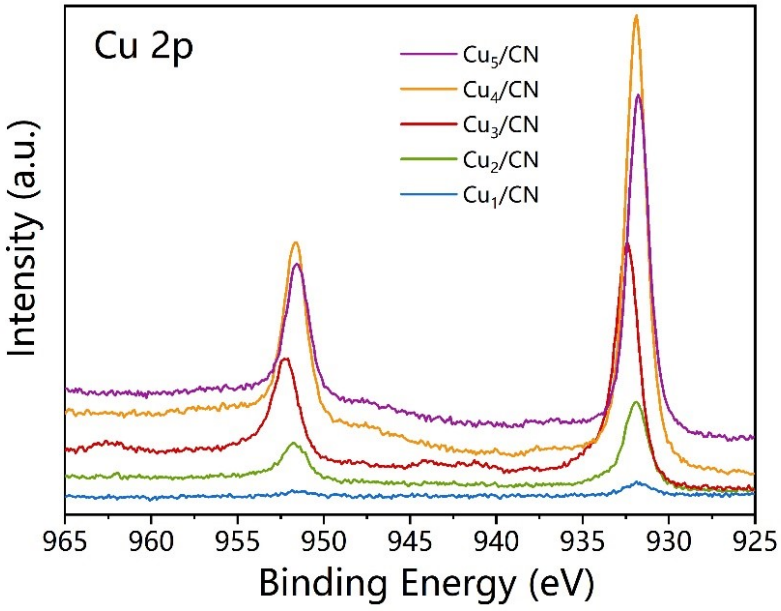

Figure S4. High-resolution XPS spectra of Cu 2p for Cu_x/CN sample.

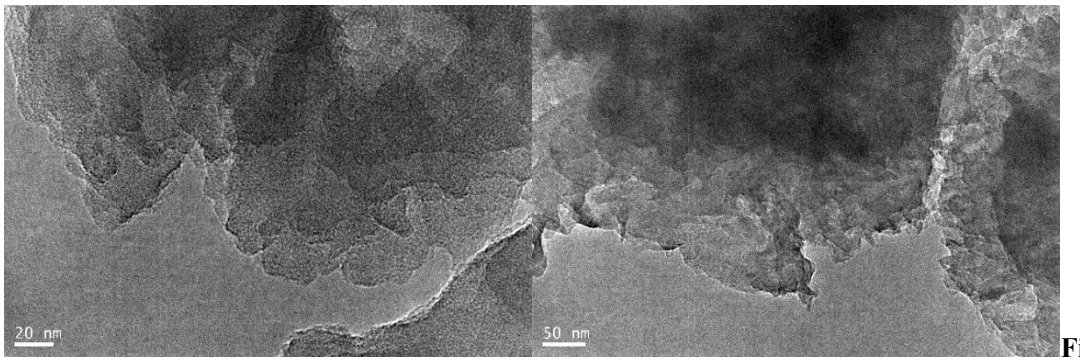

Figure S5. TEM images of g-C_3N_4.

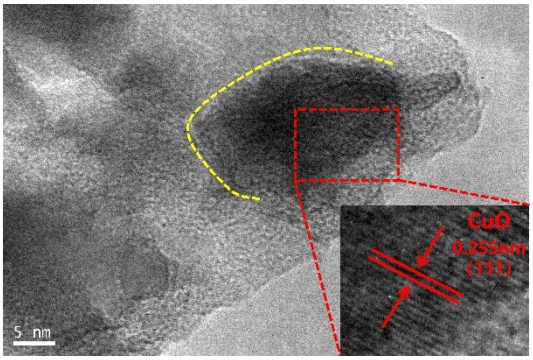

Figure S6. TEM images of Cu_3/CN.

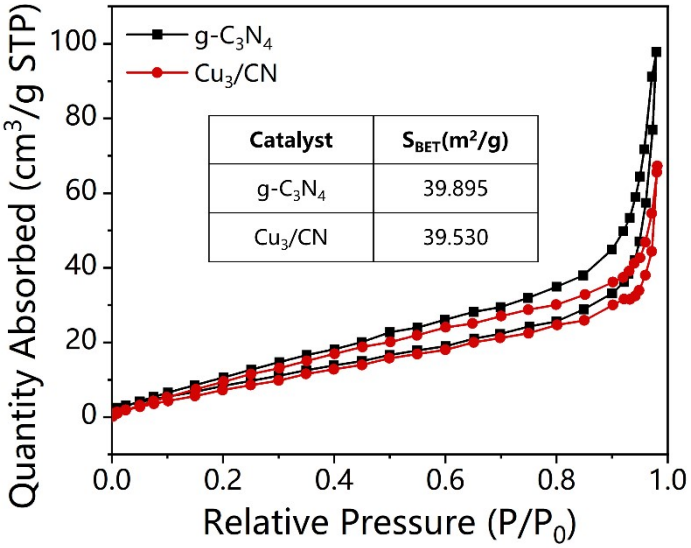

Figure S7. N_2 adsorption–desorption isotherms [Inset: Table of specific surface area].

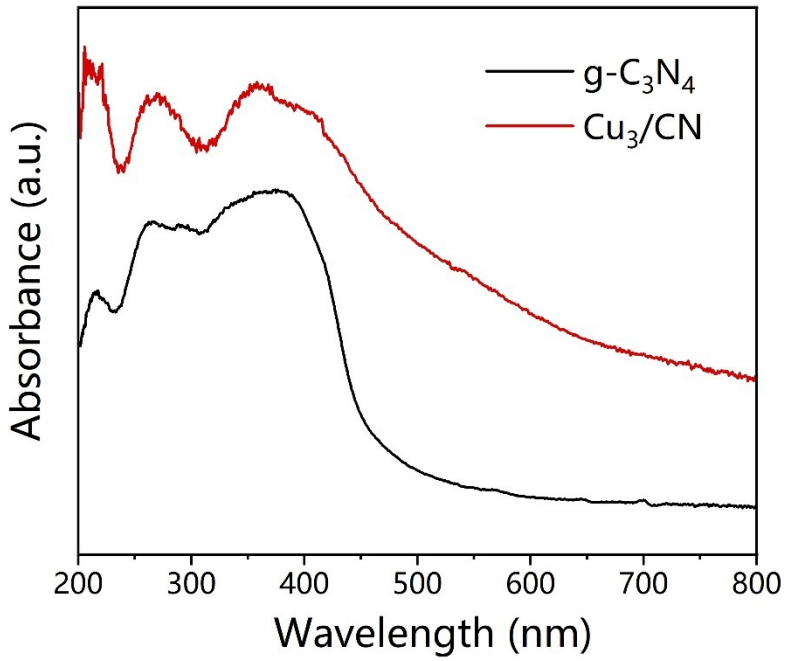

Figure S8. UV–vis absorption spectra of g-C_3N_4 and Cu_3/CN.

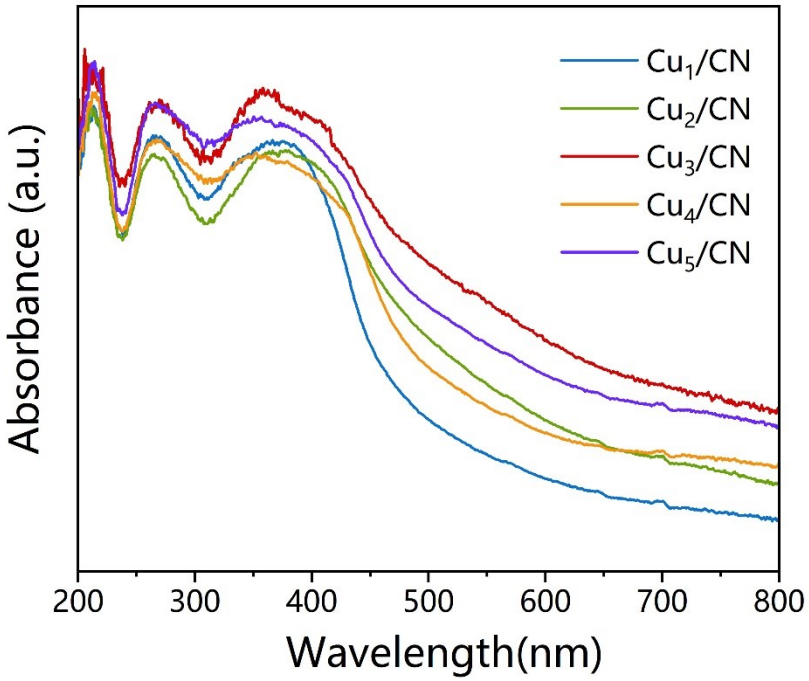

Figure S9. UV–vis absorption spectra of Cu_x/CN.

The pristine g-C_3N_4 demonstrated excellent visible light absorption at wavelengths lower than 500 nm. Moreover, the optical absorptions of all the Cu_x/CN photocatalysts are higher than that of the bare g-C_3N_4 photocatalyst. These results indicate that the Cu_x/CN photocatalysts possessed enhanced visible-light absorption ability, which promoted the generation of electron–hole pairs.

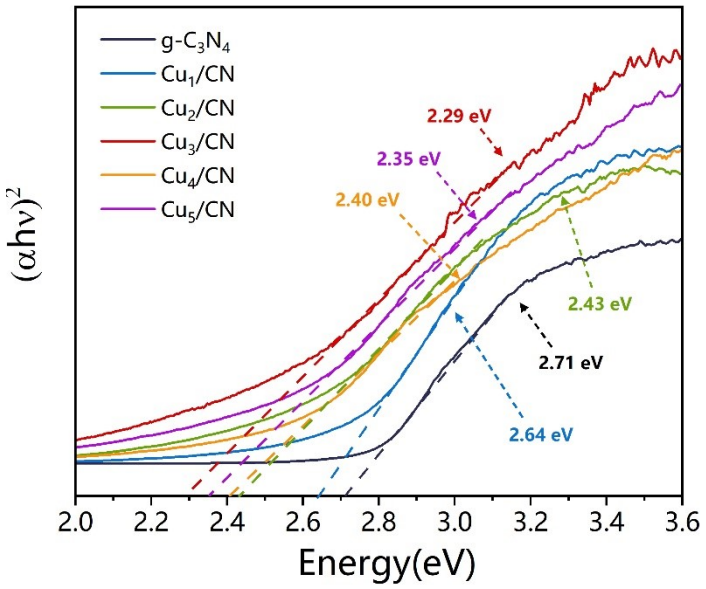

Figure S10. The plots of $(\alpha h\nu)^2$ versus $h\nu$ of g-C_3N_4 and Cu_x/CN.

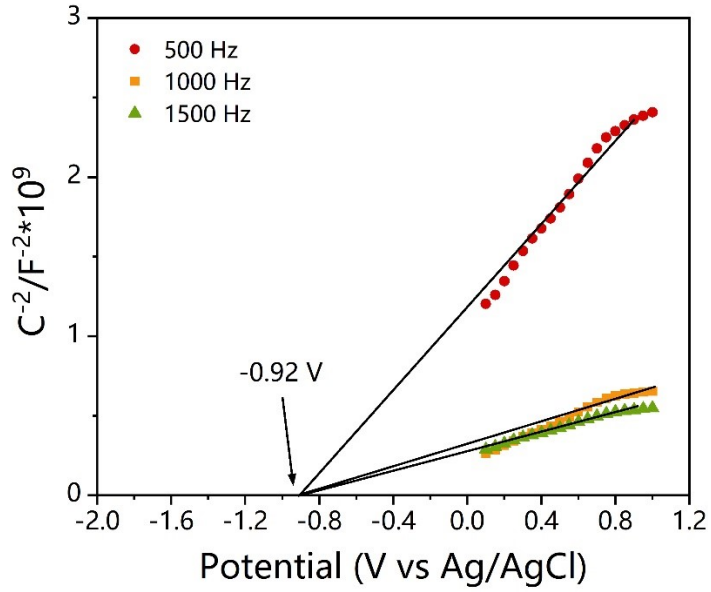

Figure S11. Mott-Schottky plots of g-C_3N_4.

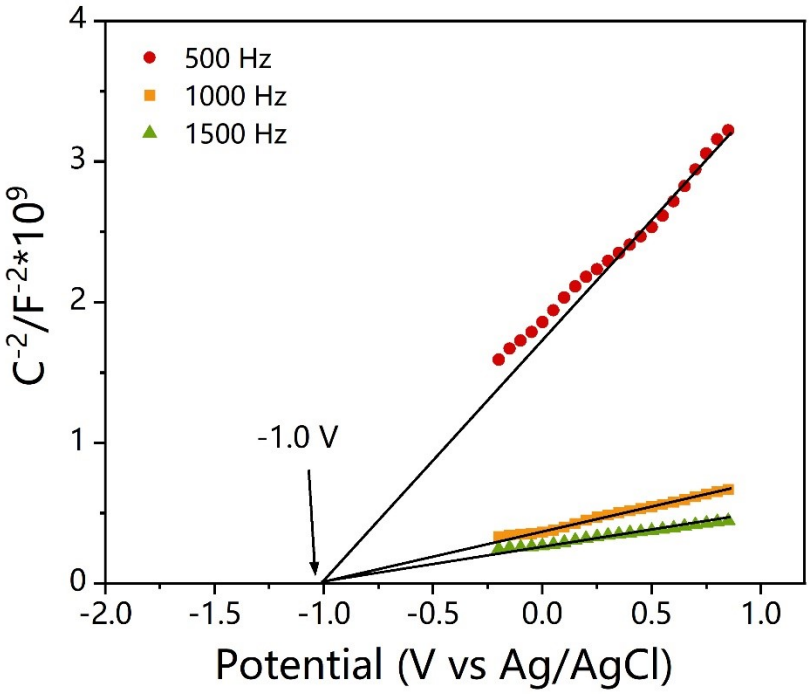

Figure S12. Mott-Schottky plots of Cu_3/CN.

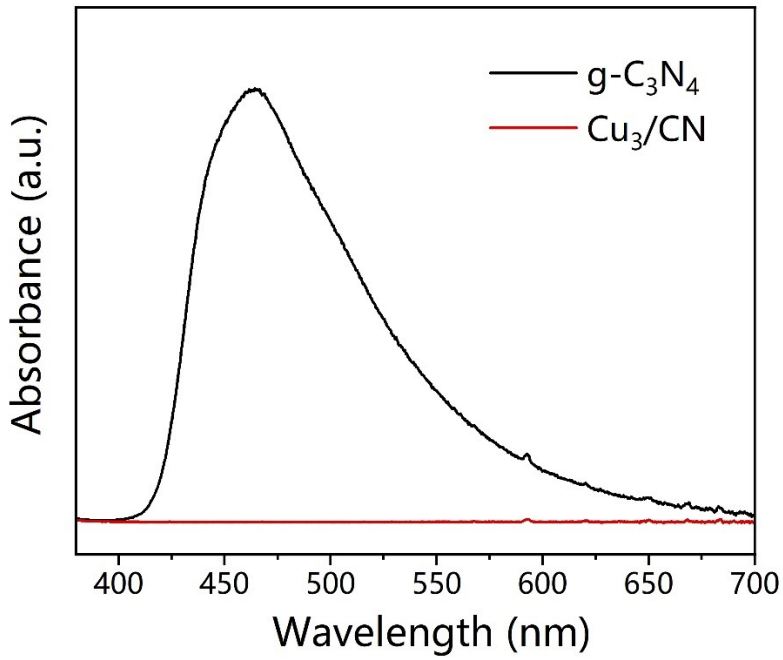

Figure S13. PL spectra of g-C_3N_4 and Cu_3/CN.

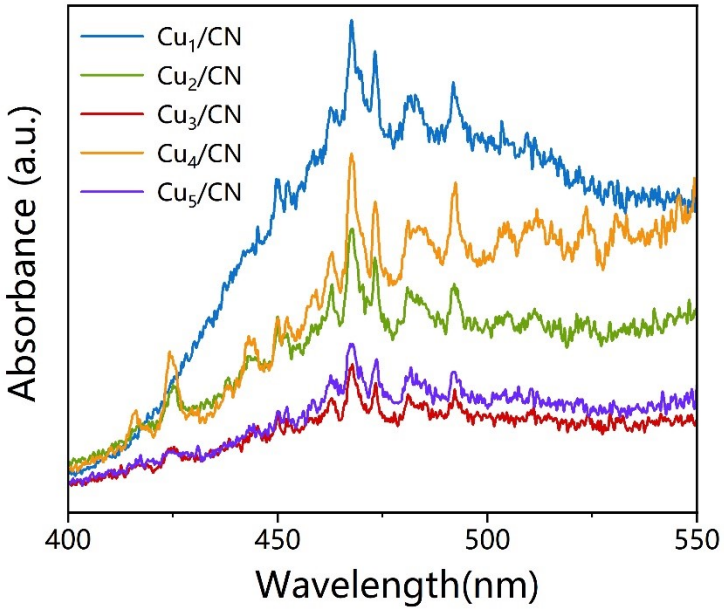

Figure S14. PL spectra of Cu_x/CN sample.

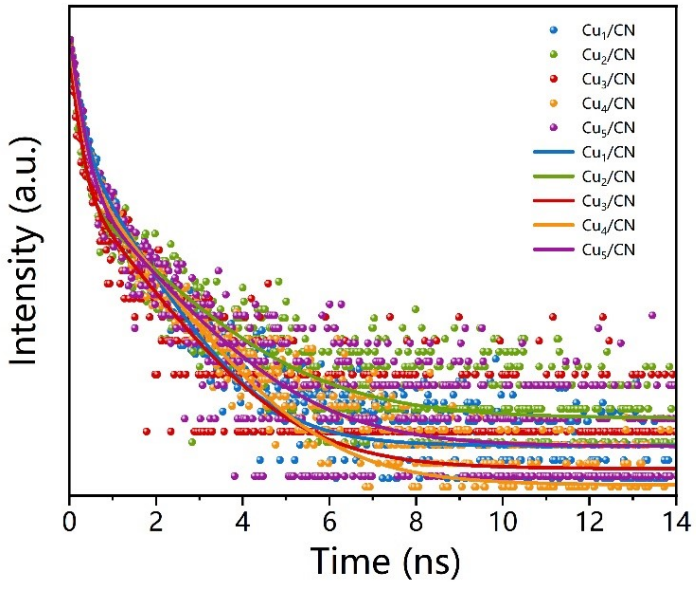

Figure S15. Time-resolved photoluminescence (TRPL) spectra.

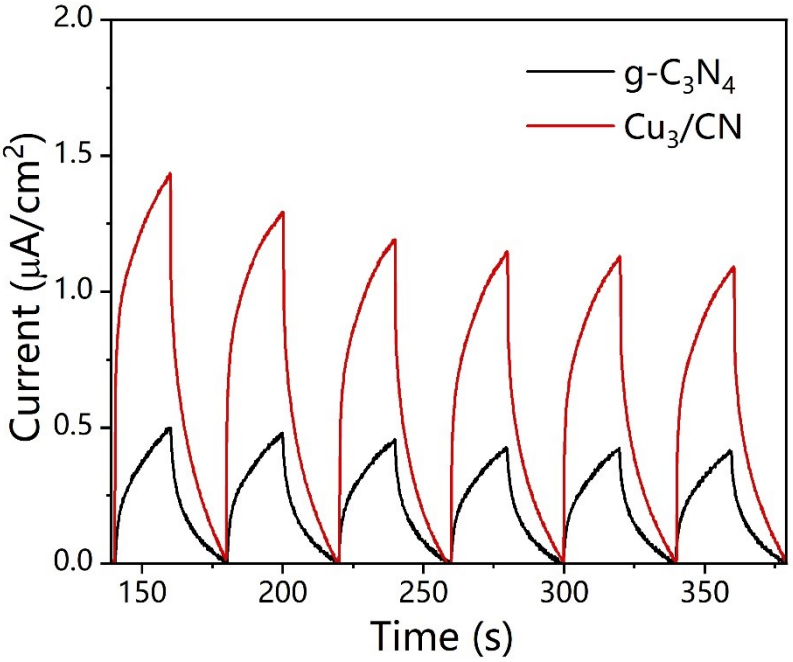

Figure S16. Photocurrent response spectra of g-C_3N_4 and Cu_3/CN.

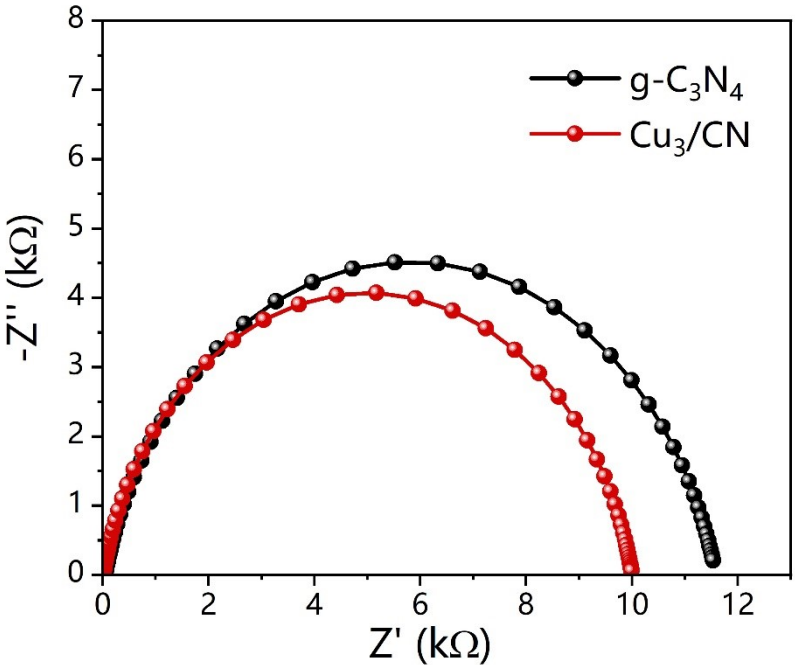

Figure S17. Electrochemical impedance spectra of g-C_3N_4 and Cu_3/CN.

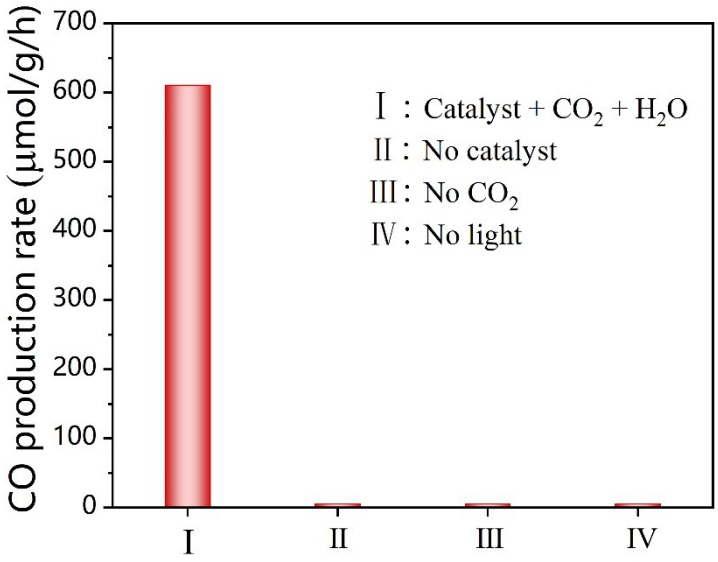

Figure S18. Control experiments of photocatalytic CO_2 reduction performance over Cu_3/CN.

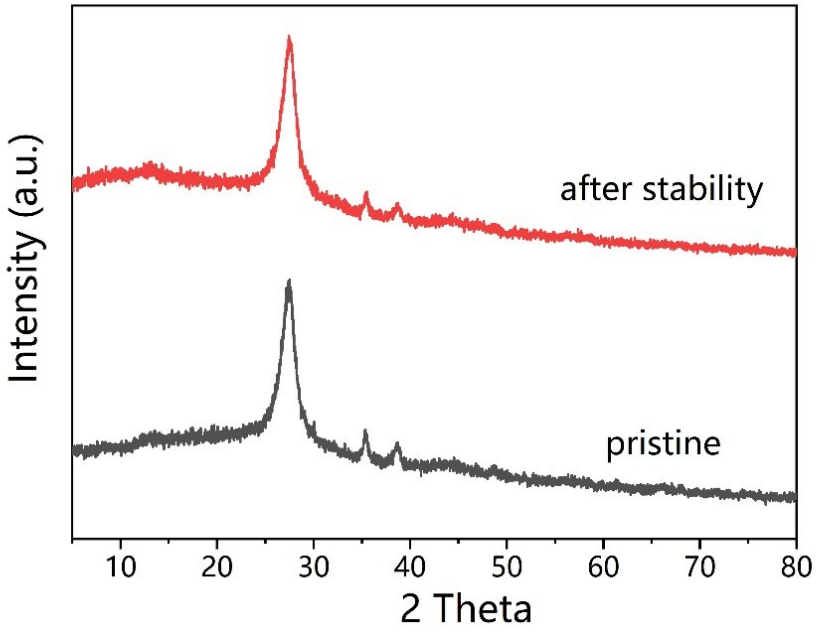

Figure S19. XRD pattern of the used Cu_3/CN.

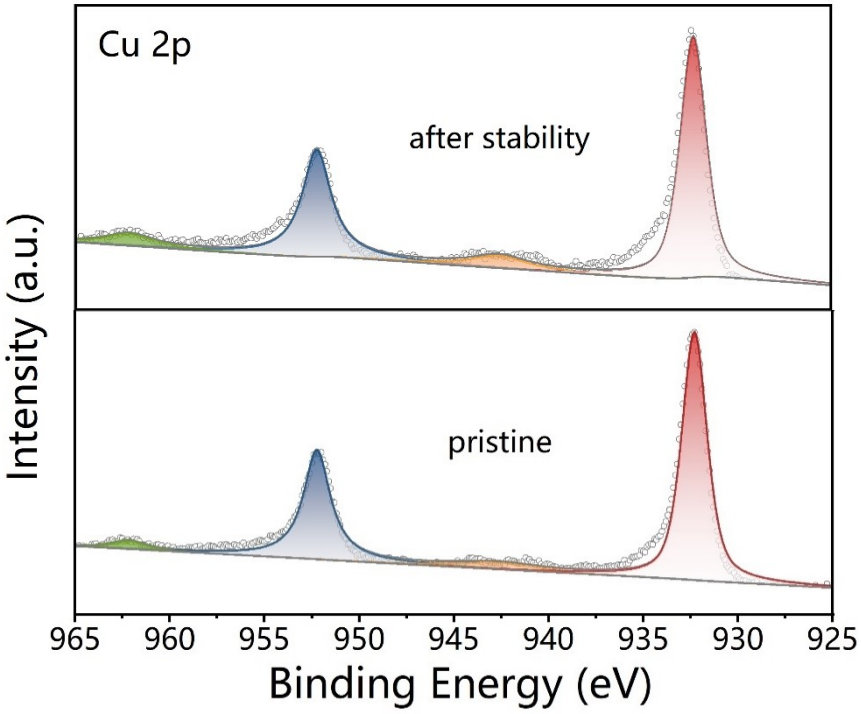

Figure S20. XPS of Cu 2p for the used Cu_3/CN.

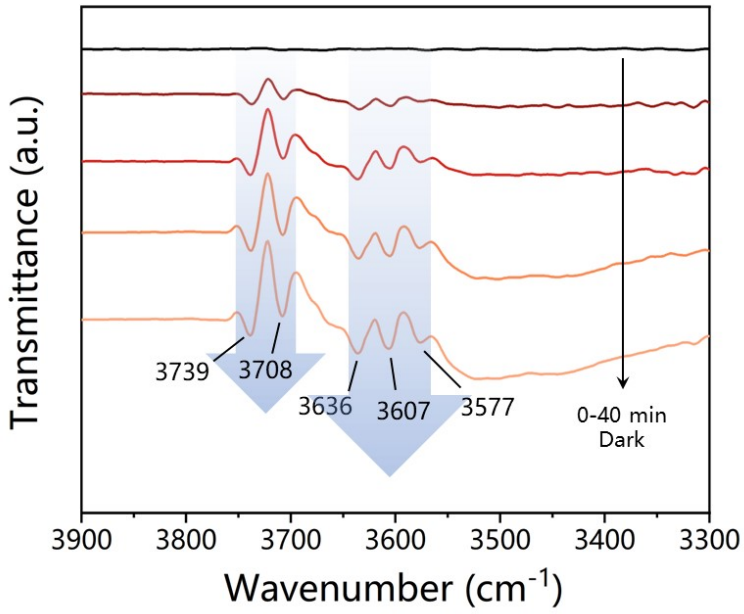

Figure S21. In situ DRIFTS test for CO_2 and H_2O interaction with Cu_3/CN in dark.

The peaks at 1672 and 1650 cm^{-1} are attributed to active $\cdot CO_2^-$ intermediates, while the peak at 1510 cm^{-1} is due to the characteristic vibrations of monodentate carbonates (m-CO_3^{2-}). The formation of bidentate carbonate ions (b-CO_3^{2-}) is confirmed by the peaks at 1541, 1377, and 1154 cm^{-1}. The absorption bands near 1635 and 1438 cm^{-1} correspond to bicarbonate HCO_3^- species, which originate from the surface-bound interactions between the adsorbed CO_2 and Cu_3/CN and are considered important intermediates. Figure 4b and S18 show the characteristic CO_2 adsorption bands with peaks centered at 3739–3577, 2362, and 2336 cm^{-1}, whose intensities indicate the CO_2 adsorption capacity of Cu_3/CN.

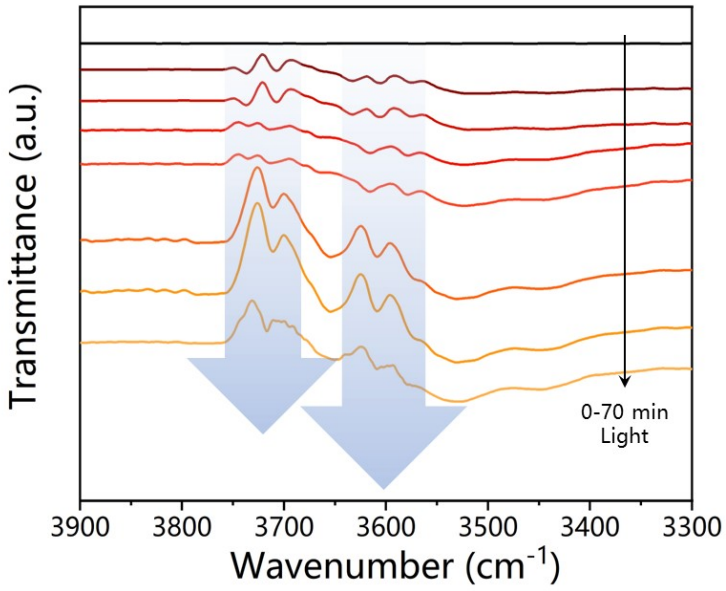

Figure S22. In situ DRIFTS test for CO_2 and H_2O interaction with Cu_3/CN under subsequently light irradiation.

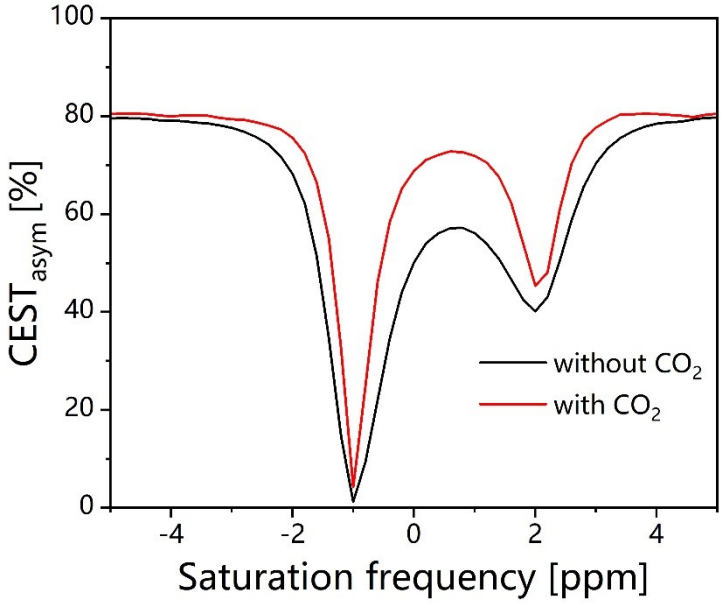

Figure S23. Z-spectra of g-C_3N_4 catalyst aqueous solution at different pH.

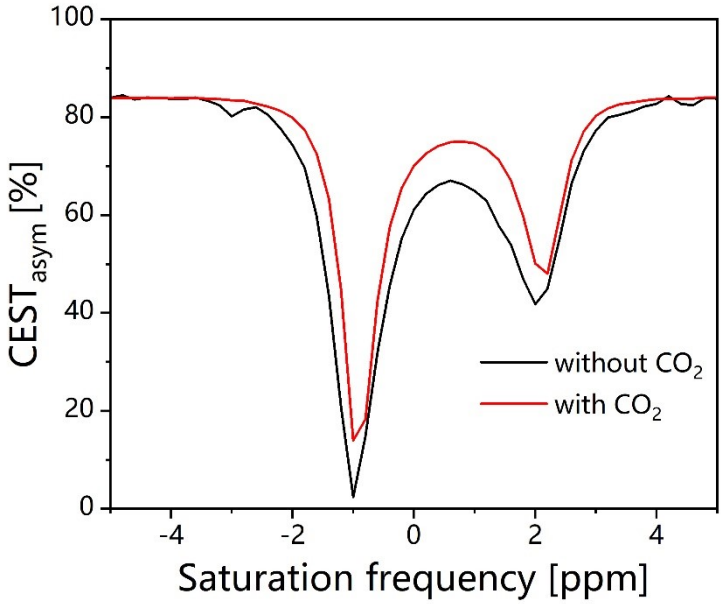

Figure S24. Z-spectra of Cu_3/CN catalyst aqueous solution at different pH.

Table S1. Copper content of Cu_x/CN.

	Weighing mass (g)	Constant volume (mL)	The measured concentration of Cu (μg/mL)	Cu final concentration (%)
Cu_1/CN	0.0530	50	20.40	1.92
Cu_2/CN	0.0473	50	73.20	7.74
Cu_3/CN	0.0591	50	168.90	14.29
Cu_4/CN	0.0526	50	212.00	20.15
Cu_5/CN	0.0480	50	208.40	21.71

Table S2. Fluorescence lifetime and average lifetime results for different samples.

Samples	τ_1(ns)	A_1	τ_1 (ns)	A_2	τ_{ave} (ns)
g-C_3N_4	0.71	0.59	3.12	0.42	2.54
Cu_1/CN	0.20	0.75	1.13	0.29	0.84
Cu_2/CN	0.16	0.81	1.78	0.16	1.27
Cu_3/CN	0.17	0.69	1.39	0.17	0.99
Cu_4/CN	0.20	0.78	1.40	0.22	1.00
Cu_5/CN	0.21	0.90	1.58	0.18	1.03

Table S3. Comparison of photocatalytic reduction of CO_2 reaction performance of CuO/g-C_3N_4 system.

Composite	Reaction medium	Light source	Activity	Reference
CuO/g-C_3N_4	H_2O	300 W Xenon lamp ($300 < \lambda < 1100$ nm)	CO: 3.7855 ($\mu mol\ g^{-1}$)	1
g-C_3N_4/CuO@ MIL-125(Ti)	H_2O	300 W Xenon lamp ($\lambda = 420$ nm)	CO: 180.1 CH_3OH: 997.2 CH_3CHO: 531.5 CH_3CH_2OH: 1505.7 ($\mu mol\ g^{-1}$)	2
CuO@SrCN	H_2O	300 W Xenon lamp ($200 < \lambda < 1100$ nm)	CO: 1.87 ($\mu mol\ g^{-1}h^{-1}$)	3
CuO/g-C_3N_4	MECN, TEOA, H_2O	3000 W Xenon lamp	CO: 5.38 CH_4: 18.61 ($\mu mol\ g^{-1}h^{-1}$)	4
CuO/g-C_3N_4	DMF, H_2O	300 W Xenon lamp	CO: 610.57 ($\mu mol\ g^{-1}h^{-1}$)	This work

References

1. M. Li, Y. Wu, E. Gu, W. Song and D. Zeng, *Journal of Alloys and Compounds*, 2022, **914**, 165339.
2. N. Li, X. Liu, J. Zhou, W. Chen and M. Liu, *Chemical Engineering Journal*, 2020, **399**, 125782.
3. A. Raza, A. A. Haidry, Z. Yao, M. F. Saleem, A. A. Alothman and S. Mohammad, *Chemical Engineering Journal*, 2024, **480**, 148162.
4. B. Yang, Y. Li, X. Yang, D. Wang, Z. Wang, E. Han and Y. He, *Solid State Sciences*, 2023, **144**, 107304.